Catalogue-Wide Satellite Photometric Behavior Paradigms

M.D. Hejduk
SRA International

ABSTRACT

Few categorization approaches for satellite photometric response as constructed from individual point-photometry measurements have been proposed; and as this is the largest and most typical photometry-collection approach, the discipline is in need of a taxonomy for the different photometric response types. The Joint Space Operations Center (JSpOC) photometric modeling approach offers an opportunity to define categories of response, as it calculates a number of parameters in applying both deterministic and stochastic models in order to predict expected satellite brightnesses. In examining these calculated parameters, a subset show promise in both identifying pathological cases and separating the more mainstream response into natural categories. A successive application of four nested tests is proposed in order to place satellites into basic photometric response types.

1. INTRODUCTION

The discipline of satellite photometry presently lacks a robust set of categories to use to characterize satellite brightness response. Recent work with satellite light curves, such as that of Payne *et al.* [1], has demonstrated the breadth of different response possibilities and shown them to be represented satisfactorily as functions of solar phase angle and solar declination angle (at least for the GEO case); but such work has stopped short of actually developing paradigmatic categories over a broad range of orbital regions and object types. It is additionally not clear whether such categories would transfer easily to a "synthetic" light-curve situation in which the response is an amalgamation of single-point measurements rather than one long, continuous track. In the asteroid tracking community, Bowell and Lumme [2] have proposed a two-parameter brightness response model, in which one parameter is the zero-phase brightness and the other scales a fixed, phase-based disillumination function; such an approach is not conceptually dissimilar to the common method of considering each satellite to have the properties of a diffuse sphere and to adjust the albedo and sphere diameter in order to create a best-fit to the observed data. Work by Lambert [3,4], Hejduk [5], and Lambour [6,7], among others, has shown the diffuse sphere assumption to be a poor model for spacecraft brightness response, certainly to anything other than the first order. Many databases simply opt for descriptive statistics of the entire photometric dataset for each satellite, prescinding from any direct attempt to model the brightness response as a function of illumination geometry. These present practices do not provide a particularly encouraging foundation for the development of brightness response paradigms for collections of single-point photometry data on individual objects.

The largest dataset of single-point photometry data is currently maintained by the Joint Space Operations Center (JSpOC) at Vandenberg AFB, CA. Consisting of all of the photometric measurements made with each metric observation, the database contains approximately 3.5 million track-averaged measurements on objects in the general satellite catalogue. These measurements feed a model to predict satellite brightness as a function of illumination geometry. This model, called KOI (Kriging Optimized Interpolation), comprises a deterministic and stochastic portion in the hopes of taking advantage of the portion of the response that can be reasonably modeled deterministically while recognizing that this portion of the model will often fall short of a satisfactory fit, thus requiring a stochastic portion, as a function of solar phase angle and solar declination angle, to try to characterize and model the residual [8]. This allows both the calculation of minimum-variance estimates of the residual at each illumination geometry point and the predictive force of the deterministic model both to be in play for a single satellite. For some satellites, the deterministic model is quite representative, and the stochastic model assumes a very small role; for others, the deterministic model is poorly representative, and the stochastic model thus has the more important job of trying to characterize and form predictions based on the residuals. When photometric data on a satellite are sparse or heavily regionalized, the deterministic model becomes important as a predictive faculty, although the Kriging stochastic model is designed to resist the usual problems with stochastic representations of sparse or regionalized data. When photometric data are dense and broadly represent the range of illumination geometries, then most interpolation schemes will perform adequately, so the precise form of the stochastic model is no longer so important.

The specifics of the KOI model and its performance have been reported and documented in other venues [8,9] and need not be given expansive presentation here; the present interest is to determine whether some of the parameters and calculations performed by this modeling effort may be useful in establishing categories of different satellite photometric response. While the KOI model is inherently flexible enough to allow deterministic models to be swapped out at an analyst's will, the present form of the model that is used is a function merely of solar phase angle; so fit results from the application of the deterministic model may outline how well parameters of a phase-angle-based function may serve as categorization criteria. The stochastic portion attempts to establish, once the deterministic portion has been removed, the remaining degree of brightness correlation with small changes in phase and declination; parameters derived from this investigation also suggest themselves as mechanisms for establishing categories of different response types. The treatment here will thus step through each proposed parameter type, examining it as a potential category boundary and, if it appears promising, suggesting actual values to use for such a boundary definition.

2. DATASET

The datasest used by the JSpOC for satellite photometric modeling is collected by the GEODSS system, a network of meter-class telescopes located at Socorro, NM; Maui, HI; and Diego Garcia, British Indian Ocean Territory. Open-aperture brightness estimates, calibrated against a sub-catalogue of main-sequence registration stars, are made as part of the frame processing for each streak. This has permitted a database of some 3.5 million photometric measurements, against a wide variety of satellite classes and orbit types, to be collected over the last several years.

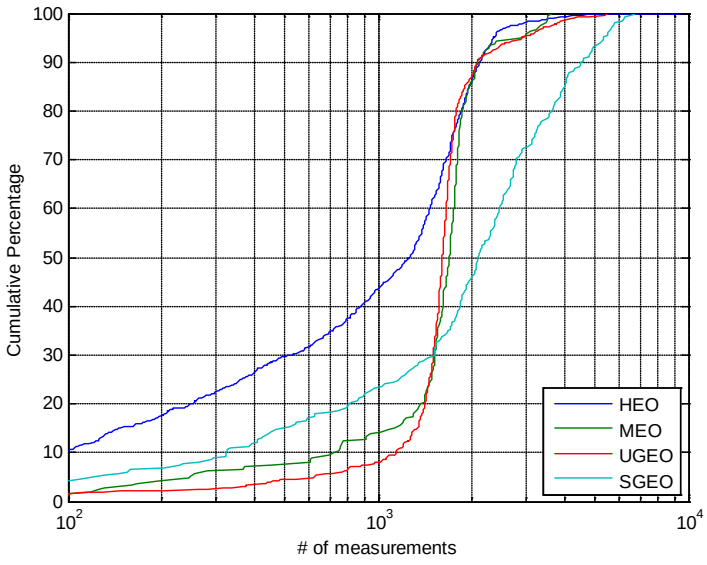

Fig. 1: Brightness measurement data densities by orbital regime

It was seen as expedient to conduct the analysis separately by both orbit class and object type. Only deep-space satellites (period greater than 225 minutes) were examined, and among these three different orbit classes were considered: HEO, with an eccentricity greater than 0.25; MEO, with a period between 600 and 800 minutes and an eccentricity less than 0.25; and GEO, with a period between 1300 and 1800 minutes, an inclination less than 35 degrees, and an eccentricity less than 0.25. The data on satellites in these orbital regimes were further separated by object type, using the categories of payload, rocket body, and debris. For the GEO orbital regime, the payload object type was further separated into station-kept (geosynchronous drift rate less than 0.03 degrees/day, called "SGEO") and "un-station-kept" (larger drift rate, called "UGEO"). Fig. 1 gives a CDF plot of the number of photometric measurements for the objects in each of these orbit regimes. In order to ensure that category conclusions be derived from adequately-sampled cases, only those satellites with measurement histories exceeding 500 measurements were used in the subsequent analysis.

3. HALF-PLANE SLOPE ANOMALOUS BEHAVIOR

The deterministic model applied as the first part of the KOI process is a linear fit to the brightness data as a function of solar phase angle. A notable body of work has concluded that the linear fit is the best simple functional representation of spacecraft brightness variation with phase angle [6, 7, 10]. While the particular phase-based approach used here is not new, there are some subtleties that set it apart from other implementations. First, a signed phase angle rather than simply an absolute value is used; negative phase is the phase angle before the minimum phase is reached, and positive phase is the angle after minimum phase. This distinction is important for stabilized GEO payloads; for in such cases the phase angle not only describes the amount of illumination but the east-west positioning of the illumination on the satellite, so in general a different response is expected at, say, a measurement

at -30 degrees in phase than a +30 degree measurement. The use of a signed phase angle necessitates two curve fits: one for the negative half-plane and one for the positive half-plane. This distinction introduces many possible categorization options, as the behavior in one half-plane can be compared to that of the other and potential useful categories articulated. Second, a binned approach to brightness representation is used; the brightness data are placed into three-degree phase bins (*e.g.*, -150 to -147 degrees, -147 to -144 degrees, &c.), with the median brightness value of the data in each giving the representative brightness value for that bin; only bins whose population exceeds a minimum value are used in the linear fit. This keeps the highly-sampled phase regions from dominating the fit and allows the overall fit to be more properly predictive of unsampled regions. Third, rather than least-squares fitting, a robust regression (iteratively-reweighted bisquare) approach is used. This method is more resistant to outlier corruption and therefore should serve as a better representation of behavior across the entire phase angle region. Fourth, a Student's *t*-test is performed against the derived slope from the linear fit to ensure that it differ significantly from zero, and only those cases in which the *t*-test is passed (at the 5% significance level) is the linear fit registered.

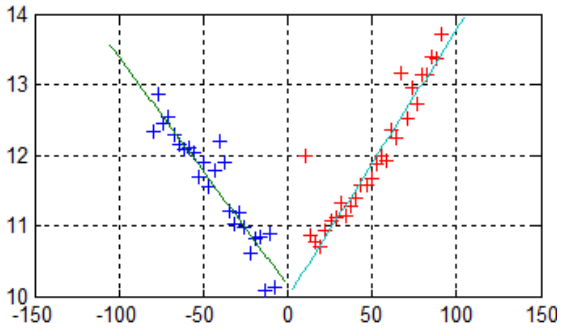

Fig. 2: Example of brightness fit versus solar phase angle. The y-axis is Mv; the x-axis is signed solar phase angle.

Fig. 2 gives an example of this fitting approach and displays a well-behaved case. Each symbol represents one brightness bin, blue for negative phase angles and red for positive phase angles. Both datasets are quite reasonably represented by a linear fit. The two fits both show a decrease in brightness with increasing (absolute value of) phase angle, and in addition are of approximately the same slope and share a near-common point of intersection with the 0-phase vertical line. This would represent the expected behavior for the typical space object, so perhaps a first test of atypicality might be a failure to conform to the broader parts of this paradigmatic behavior. Possible deviations would be the "wrong" slope, in which brightness would increase with decreasing phase angle, in one or both half-planes, or simply the failure to establish a linear fit in either or both half-planes due to the failure of the *t*-test.

Table 1 below gives a summary of such cases, broken out by orbital regime and additionally by object type. One is struck by the degree to which the paradigmatic case of a properly-sloped fit in each half-plane is observed: at least 95% of the time for each of the orbital regimes. The only instance in which a significant departure appears is that of HEO debris, in which 20% of the cases display fits with non-canonical slope. So a first grouping might be those cases that exhibit the expected behavior with phase in both half-planes. While this separates only 5% of the cases from the main group, it is clear that such situations are of a different kind and especially puzzling when well sampled.

Table 1: Linear fit anomalous conditions by orbital regime and object type. The values are percentage of each object type (each column adds to 100)

	HEO				MEO				GEO				
	Pay	R/B	Deb	Tot	Pay	R/B	Deb	Tot	Spay	Upay	R/B	Deb	Tot
Both slopes wrong			6.7	1.5						0.5		11.1	0.4
One right, one wrong		1.4	14.0	3.9	1.9	2.7		2.1	2.9	6.2	1.2	11.1	4.3
One 0, other right													
One 0, other wrong													
Both slopes zero													
Both slopes right	100.0	98.6	79.3	94.6	98.1	97.3	100.0	97.9	97.1	93.3	98.8	77.8	95.3

4. MAGNITUDE AND CONSISTENCY OF HALF-PLANE SLOPES

For those cases that conform to the paradigmatic behavior, described previously, the next area of inquiry is the magnitude of the fitted slopes themselves. The plots in Fig. 3 show these values by orbital regime and secondarily

by object type. While the graphs' x-axes are numerically delimited by slope itself (Mv / phase degree), the vertical lines are placed such that each line represents a brightness decrease of one visual magnitude over the brightness space of -105 degrees to 0 degrees (or vice versa in the positive half-plane). In examining the Fig. 3 plots, when there is a "knee" in the CDF curve it tends to occur at the second vertical line, which represents an overall difference of two visual magnitudes over the typical phase angle observing range; this is true for all of the object types in GEO, for debris in HEO, and for rocket bodies in HEO and MEO. Across all three orbital regimes, response for rocket bodies and debris is almost entirely confined to this 2 Mv region; it is payloads, both stabilized and unstabilized, that frequently stray beyond this. So if one wishes to articulate some catetorial criteria based on linear fit slope, he can begin perhaps with a slope threshold of 0.022 Mv / phase degree. This slope threshold would flag unusual debris and rocket body response across all orbital regimes, separate out about half of the payloads in HEO and GEO, and flag unusual payload response in GEO. Such a criterion never separates more than 30% of any given object type group, but it is a beginning.

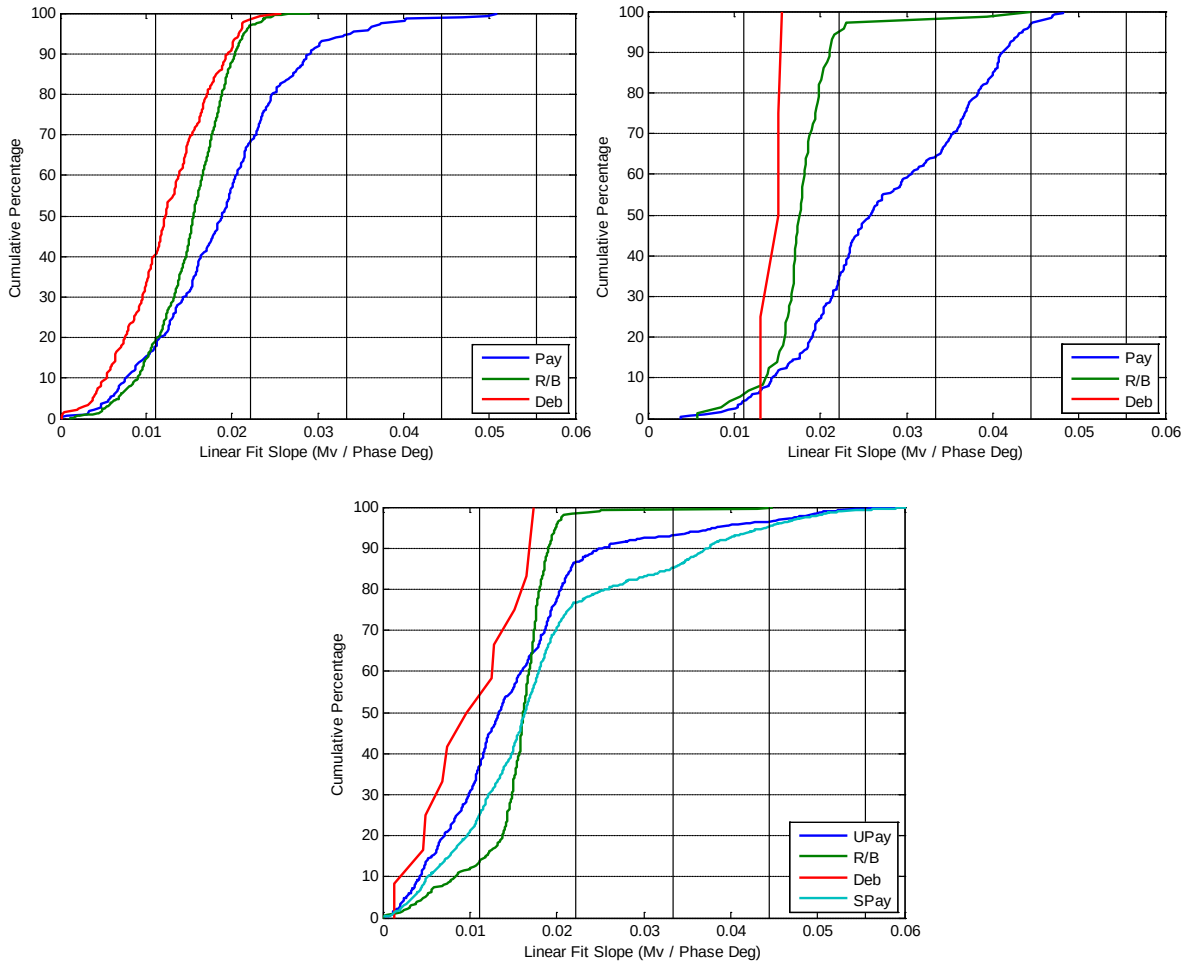

Fig. 3: CDF plots of absolute value of linear slope. Clockwise from top left: HEO, MEO, GEO

5. HALF-PLANE SLOPE SYMMETRY

An additional area of enquiry is an examination of the degree of symmetry between the slopes in the negative and positive half-planes. The expectation is that for non-stabilized objects, especially in the highly-sampled case, the random aspect function should produce nearly identical Mv-vs-slope functions for both positive and negative phase angles; stabilized payloads could well show significant differences. Fig. 4 below shows the half-plane slope differences by orbital regime and secondarily by object type. The difference value reflected in the CDF plots is

simply the sum of the negative half-plane slope and the positive half-plane slope; if the negative half-plane slope is larger, then a negative value will be produced &c. Obviously, a value near zero indicates symmetry.

For HEO and MEO, 80% of all three object types manifest absolute slope differences less than 0.005 Mv/deg; and for rocket bodies it is nearly 100%. For GEO objects, the 0.005 separator is more useful in that it contains 80% or better of rocket bodies, debris, and unstabilized payloads but only 40% of the stabilized payloads. While perhaps somewhat less cut-and-dried than the absolute slope measurement, this value still provides a reasonable categorial boundary.

In examining the graphs, a slight negative bias is observed for all three orbital regimes; it is most pronounced in GEO. This is believed to be an artifact of the manner in which GEODSS sensors respond to sensor tasking: because they wish to give themselves multiple opportunities to track an assigned satellite should acquisition fail on the initial attempt(s), they schedule each object shortly after it enters the sensor's FOV, which for most objects (especially in GEO) corresponds to a negative phase angle. Because of this scheduling favoritism, the negative half-plane tends to get denser and broader sampling than the positive half-plane, which can give rise to the kind of bias observed here.

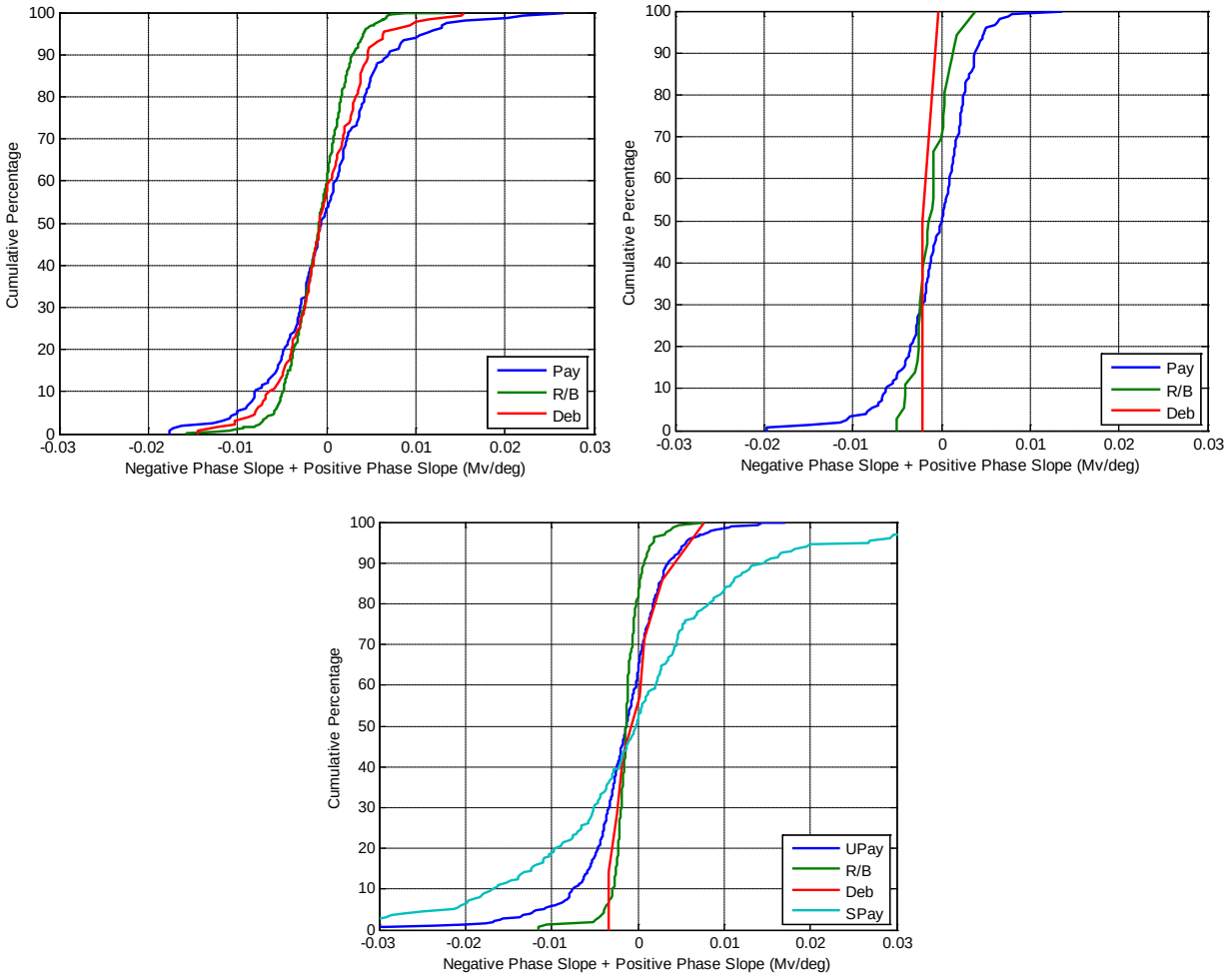

Fig. 4: Differences in slopes of linear fit in each half-plane. Clockwise from top left: HEO, MEO, GEO

6. STANDARD ERROR OF LINEAR FIT

A final potential discriminator among response types is the standard error of the linear fit. Since robust regression is used, the standard error is changed from the usual calculation (appropriate when the sum-of-squares residual is being minimized) to the mean absolute deviation, here divided by a constant to render it an unbiased quantity for the normal distribution.

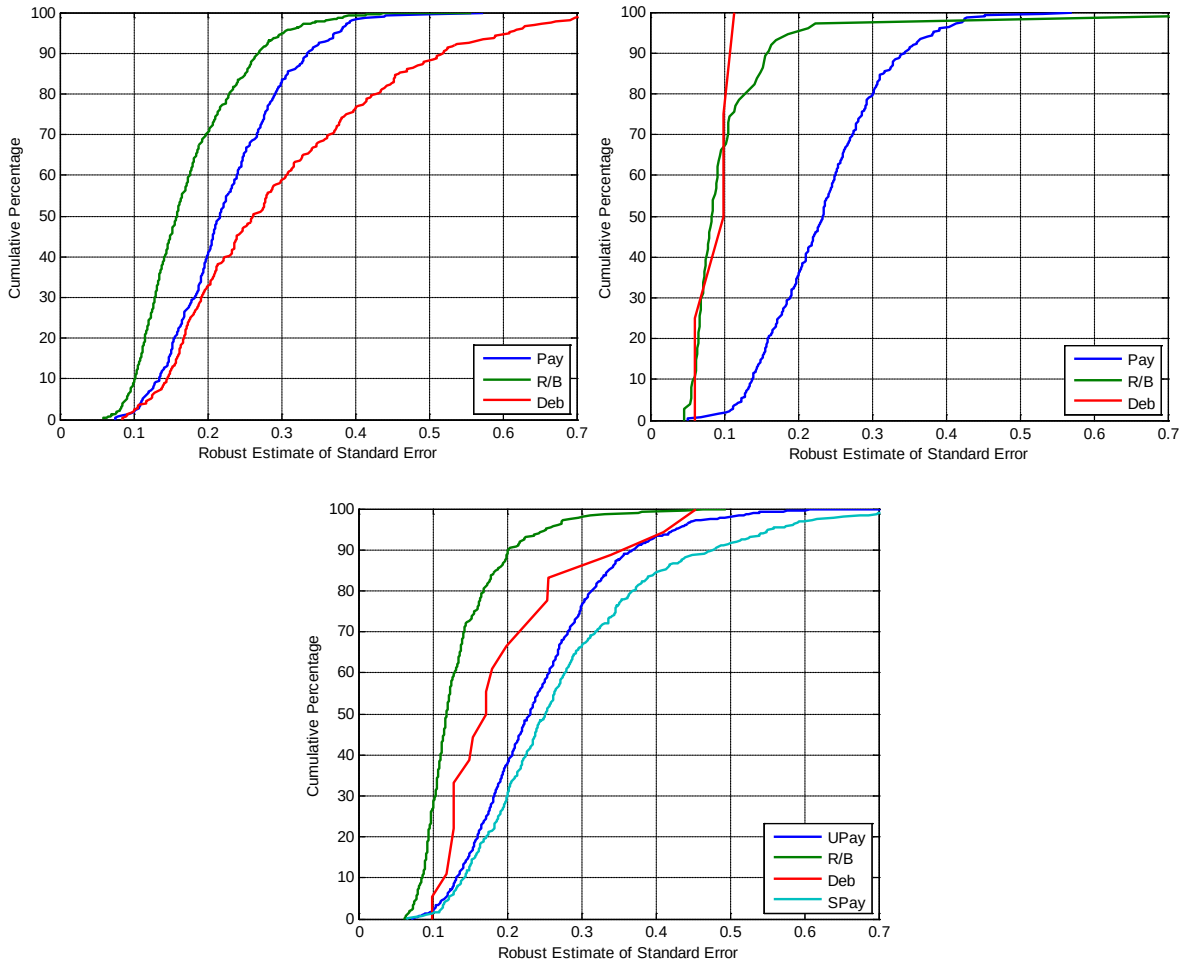

Fig. 5: Robust estimate of fit standard error. Clockwise from top left: HEO, MEO, GEO

Fig. 5 shows the results, in CDF form, for this particular quantity. In the MEO and GEO orbital regimes, rocket bodies are the best behaved (the debris sample size is small and not particularly conclusive), with at least 90% of the cases achieving a standard error value of 0.2 or smaller; payloads (of both types) exhibit much larger values: 60% of the MEO/GEO payloads have standard error values larger than 0.2. In HEO a different behavior is observed. While still the best behaved of the object types, rocket bodies now require a threshold of 0.3 in order to meet the 95% level, and debris is by far the worst performing of the object types. Because the CDF plots here are mostly continuous rather than displaying knee-type behavior, and because any choice of an arbitrary cumulative percentile threshold (e.g., 95%) would produce notably different standard error thresholds by orbit regime, it does not appear that the standard error attribute will serve well to define a response category.

As an aside, the shift in object type performance prompts an investigation of the manner in which satellites can manifest a poor standard error value; and upon visual examination of a large number of cases, it becomes clear that there are two principal strains of this behavior: large random errors and clearly systematic errors. Fig. 6 gives an example of both. Most stabilized payloads with large errors manifest them as systematic errors, varying from the

linear fit in a continuous and predictable way; most non-stabilized objects show random variation, in which there is little discernable pattern about the fit line. Such cases are easy to distinguish visually. For automatic recognition, one approach could be attempting a polynomial fit and determining whether the standard error of that fit is significantly better than that of the linear case. When this is true, a systematic deviation situation is present; when it is not, a random error situation can be presumed.

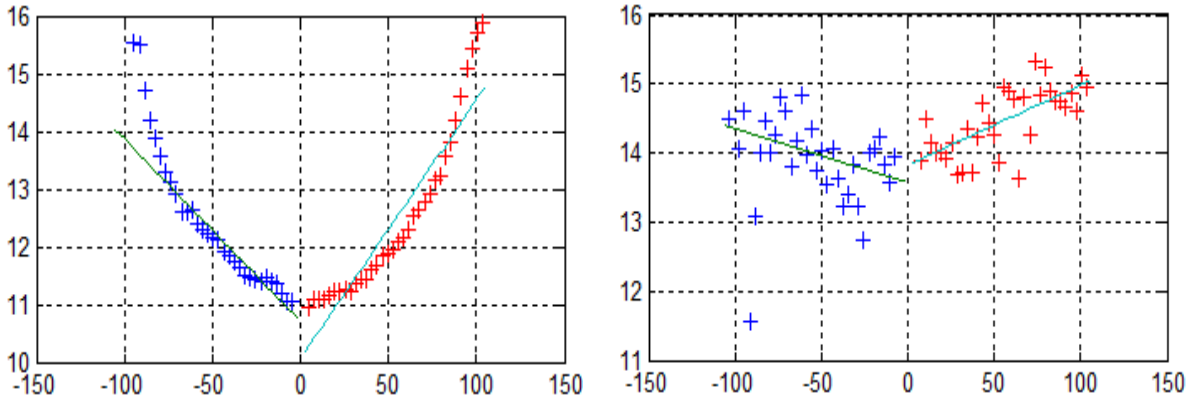

Fig. 6: Two different strains of large standard error of fit. The graph at left, showing systematic variation, is from a stabilized payload; the one at right, showing random error, is from a rocket body.

7. VARIOGRAM-RELATED PARAMETERS

It was discussed previously that the KOI brightness modeling approach employed both a deterministic and a stochastic model. The robust linear fit in phase, examined in the previous sections, constitutes the deterministic model; and if fully adequate to the task, its application should "detrend" the residual data so that there are no systematic effects in solar phase angle. This leaves a group of residuals that should manifest only stochastic dependencies in solar phase and solar declination.

A common way to evaluate such dependencies is to construct a variogram, which will characterize the change in object brightness as a function of small changes in phase and declination angle. Imagine each brightness residual plotted on a three-dimensional graph, with the brightness residual as the dependent variable (z) and the solar phase angle and solar declination angle of each residual as the independent variables (x and y). For every pair of residuals, the square of the brightness difference (γ) and the Euclidian difference between the points x-y plane coordinates (h) are calculated, these results are binned, and the binned results plotted in a manner that shows the brightness dependence as a function of phase-declination Euclidian distance. Fig. 7 gives an example of a canonical variogram, which contains several features of interest. First, this particular variogram intersects the origin, which means that brightness difference correlates with small changes in phase/declination angle all the way to the smallest variation. Had it manifested a positive y-intercept (called a "nugget" from the technique's origin in the mining industry), this would indicate a component of random error: for phase/declination changes smaller than a certain amount, the effect on brightness is essentially random; this establishes a limit on the fidelity of any predictions the model may make. Second, this variogram reaches a horizontal asymptote (called a "sill"); this outcome means that beyond a certain degree of Euclidian separation in the phase/brightness plane, there is no longer any correlation between brightness values; the separation distance for which this happens is called the correlation length and defines

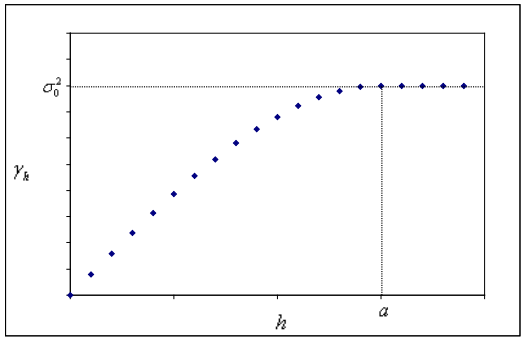

Fig. 7: Canonical stationary variogram

the region of the regionalized variable. To complete the picture, the variogram will be used as a weighting function to compute any desired predicted brightness value (as a function of solar phase and declination angles) as a linear combination of the surrounding data.

This stochastic modeling approach suggests two possible categorization parameters, and the first is whether the variogram reaches a horizontal asymptote. The presence of such an asymptote, called a "stationary" situation and of interest because it gives the stochastic solution additional desirable properties, also speaks to the deterministic model's having accounted for most of the systematic brightness. Table 2 gives the percentage results for this feature by orbital regime and object type. An "indeterminate" situation is one in which no suitable variogram model, stationary or otherwise, could be applied.

Table 2: Variogram types. The values are percentage of each object type (each column adds to 100)

	HEO				MEO				GEO				
	Pay	R/B	Deb	Tot	Pay	R/B	Deb	Tot	Spay	Upay	R/B	Deb	Tot
Stationary	77.0	69.3	74.4	72.1	68.4	56.8	50.0	66.0	82.4	75.2	66.3	44.4	74.8
Non-Stationary	10.9	14.7	19.5	14.9	14.8	10.8		13.9	8.8	13.2	7.6	44.4	11.2
Indeterminate	12.1	15.9	6.1	12.9	16.8	32.4	50.0	20.1	8.8	11.7	26.2	11.1	14.1

It is heartening to see that the stationary forms of the variogram predominate, in anywhere from two-thirds to four-fifths of the cases (debris in MEO and GEO is undersampled and therefore not definitive). In these stationary cases, the conclusion is that the deterministic model chosen (here the robust regression fit as a function of phase angle), once applied, successfully keeps the mean brightness the same throughout all of phase-declination space. The longer the variogram takes to reach the asymptote, the larger each "region" of phase-declination space needs to be in order to realize this constant mean; but there is no overall drift of the mean brightness in phase or declination. This does not mean, of course, that the linear fit model is the best model; a better model would reduce the post-deterministic brightness residuals and thus leave less of the overall prediction to the whims of the stochastic model, improving the brightness prediction reliability for any given phase-declination independent-variable pair. However, it does show that the linear fit model is frequently capable of reducing the situation to one that is truly stochastic.

Rocket bodies lodged some of the best performance with regard to the linear fitting, so it is somewhat surprising to see them fare relatively poorly in terms of producing stationary variograms. However, this poor performance does appear ironically to be brought about by the success of the fit. The post-deterministic-model residuals in such cases have been reduced to levels commensurate with the inherent errors of the observations; and in such cases, the variogram itself becomes unreliable. One thus observes the indeterminacy numbers to be higher for rocket bodies than for the other object types. Cases of non-stationarity also may be elevated, but these elevations are slight and do not in every case predominate (*e.g.,* HEO rocket bodies versus debris).

For those cases that do embrace a stationary model, one is next interested in the ratio of the y-intercept value to the asymptote value. If this value is large, then there are large changes in brightness correlation with Euclidean separation distance; if it small, then there actually is not much correlation at all with Euclidean distance, meaning that the brightness residuals essentially vary randomly (as opposed to a correlated manner with phase and declination angles).

The results are shown in Fig. 8. Perhaps as expected (given the stationary / non-stationary performance observed previously), rocket bodies in all three orbit regimes yield the least correlation with phase and declination angles, as shown by the high percentage of y-intercept-to-asymptote values—nearly all greater than 80%. As was explained previously, this appears to be due to the linear fit's consistently good performance against this object type: the residuals are essentially random and show no further correlation with the independent variables used. The other object types show a wider range of this percentage, although there is no obvious "knee in curve" that would separate one type of response from another. The curves do produce a left-skewed tail, but even this is approached more or less continuously. One could say, for example, that the MEO payload line changes character at about the 70% point, but this would be a distinction more arbitrary than definitive; and such thresholds would have to be set separately for each object type within each orbital regime; it is not easy to articulate a single standard that would suffice for multiple regimes and types.

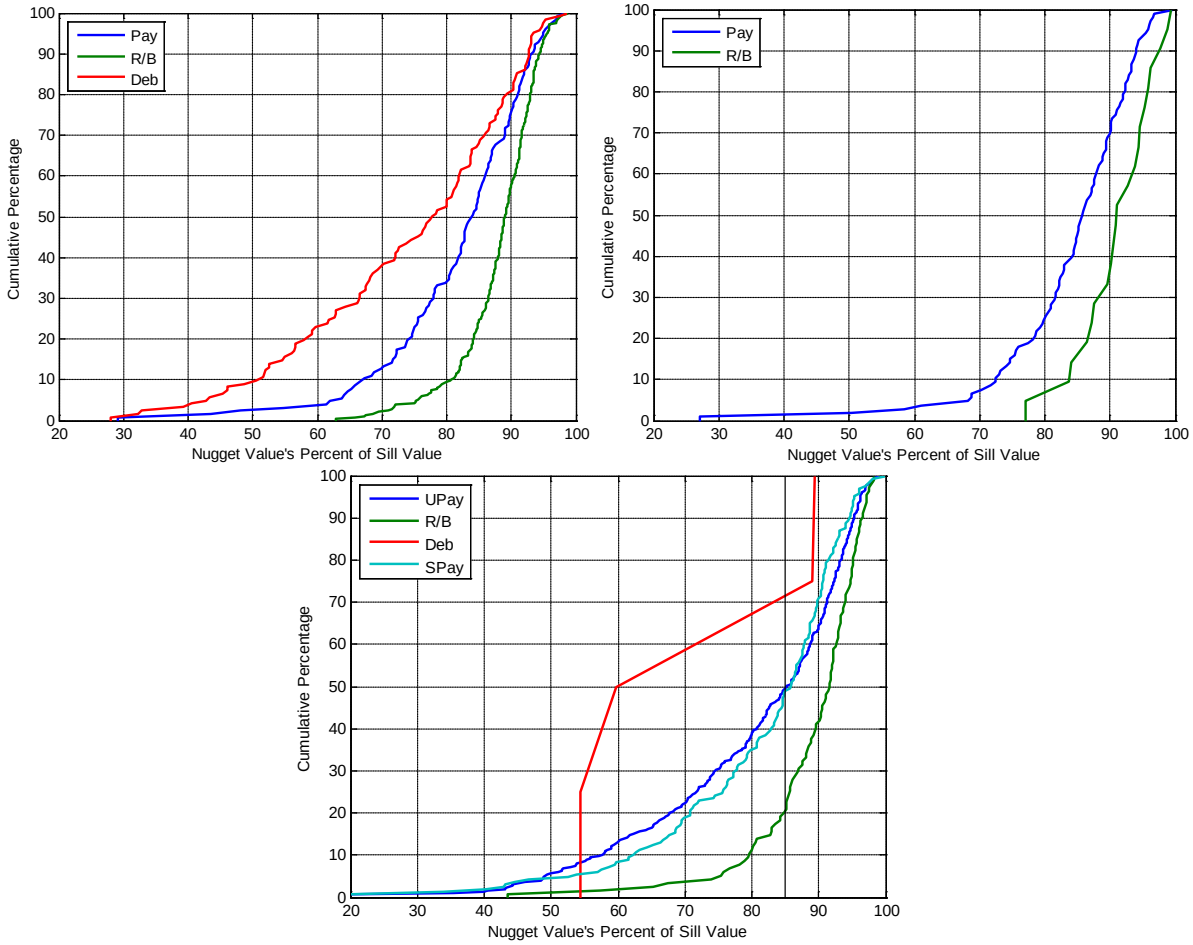

Figure 8: Ratio of variogram y-intercept (nugget) to asymptote (sill)

7. CATEGORIZATION SUMMARY

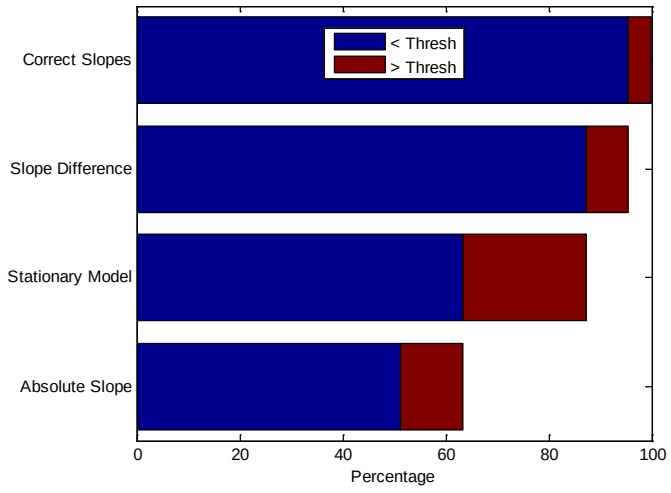

Figure 9: Results of successive application of categorization criteria

The preceding sections have outlined and evaluated possible categorization parameters and, in those cases in which the parameters seem promising, have recommended actual threshold values that will act to separate out different kinds of response. In trying to present the result of a contemporaneous application of the promising parameters, one is faced with a large number of possible combinations. Fortunately, a simplification is at hand in that the parameters themselves suggest a nested application: one would first want to screen for "abnormal" slopes as the most basic of normality investigations, then apply the slope symmetry test to the cases that survive the abnormal slope test as an indicator of an abiding satellite

asymmetry, then apply the stationarity test to the cases that survive the slope symmetry test as an indicator of the adequacy of the overall linear model, then separate this last set into small and large absolute slopes as a simple division of this remaining sample space. Fig. 9 shows the results of this successive application of tests. The first three categorizations successively identify and eliminate minority and pathological cases: the correct slopes test eliminates about 5% of the cases, the slope difference test eliminates about 8%, and the stationary model test eliminates about 24%. The absolute slope test separates the remainder into a 12% and a 51% set. So the successive application of these criteria creates five different categories, with the four small categories ranging from 5% to 24% and the remaining "mainline" category with about half of the overall cases. While one might wish for a broader categorization of the full response set, rather than leaving half of the cases as a main-sequence group, on the whole this categorization approach is not unattractive. Each of the divisions maps to an attribute useful for brightness modeling, and the thresholds used respond to the "knees-in-the-curve" for each such attribute. More study would be necessary to determine how best to divide up the main-sequence set, but it is expected that binning of a more or less arbitrary kind might be required. Furthermore, at some point it should be investigated how well these categories can be brought to bear on the more lightly-sampled cases (i.e., those with fewer than the 500 measurements required for this study) and whether they break down at a certain sample size.

It is interesting that three of the four categorization criteria make use of a functional dependence on solar phase angle only, and the one exception (stationarity) can revert to this if the dependence on solar declination angle is weak. This analysis thus testifies to the enduring utility of phase angle as a broad-spectrum brightness classifier, despite its known limitations.

8. REFERENCES

1. Payne, T.E., Gregory, S.A., Tombasco, J., Luu, K., Durr, L., "Satellite Monitoring, Change Detection, and Characterization using Non-Resolved Electro-Optical Data from a Small Aperture Telescope", 2007 AMOS Technical Conference, Kihei, HI, 2007.
2. Bowell, E. and Lumme, K. "The IAU Two-Parameter Magnitude System for Asteriods," *Asteroids II*, Edited by Binzel, R., Gehrels, T, and Matthews, M., Tucson, AZ: The University of Arizona Press, 1982.
3. Lambert, J.V., "Interpretation of Geosynchronous Satellite Phase Angle versus Magnitude Relationships", Contract F05603-90-C-0010 Specialized Data Report: MOTIF FY95-01, 30 NOV 1994.
4. Lambert, J.V., "Analysis of Magnitude versus Phase Angle Data for Two Classes of Deep Space Satellites", Contract F05604-95-C-9011 Specialized Data Report: MSSS FY96-04, 11 OCT 1996.
5. Hejduk, M.D., Kervin, P.W., Lambert, J.V., Stansbery, E.G., Africano, J.L, and Pearce, E.C., "Visual Magnitude Satellite Catalogue Release 1.0", 2001 AMOS Technical Conference, Maui HI, SEP 2001
6. Lambour, R.L., "Phase Angle Dependence of Satellite Brightness Derived from Space-Based Visible Data", MIT/LL Project Report SPC-8, 20 FEB 2001.
7. Lambour, R.L. and Sayer, R.W., "ETS Measurements of Satellite Phase Curves at High Phase Angles", MIT/LL Project Report ETS-138, 12 SEP 02.
8. Okada, J.M. and Hejduk, M.D. "Satellite Brightness Estimation using Kriging Optimized Interpolation." 2005 AMOS Technical Conference, Kihei, HI. September 2005.
9. Hejduk, M.D., "Satellite Photometric Modeling using Kriging Optimized Interpolation (KOI)." AFSPC/A9A Technical Report, 1 SEP 09.
10. Hejduk, M.D. "Phase Functions of Deep-Space Orbital Debris." 2007 AMOS Technical Conference, Kihei, HI. September 2007.